Space Weather

RESEARCH ARTICLE
10.1029/2022SW003243

Amplitude Scintillation Severity and Fading Profiles Under Alignment Between GPS Propagation Paths and Equatorial Plasma Bubbles

J. Sousasantos[1], B. J. Affonso[2], A. Moraes[3], F. S. Rodrigues[1], M. A. Abdu[2,4], L. A. Salles[2], and B. C. Vani[5]

[1]William B. Hanson Center for Space Sciences, University of Texas at Dallas (UTD), Richardson, TX, USA, [2]Instituto Tecnológico de Aeronáutica (ITA), São José dos Campos, Brazil, [3]Instituto de Aeronáutica e Espaço (IAE), São José dos Campos, Brazil, [4]Instituto Nacional de Pesquisas Espaciais (INPE), São José dos Campos, Brazil, [5]Instituto Federal de Educação, Ciência e Tecnologia de São Paulo (IFSP), Presidente Epitácio, Brazil

Key Points:

- Space weather impacts on Global Navigation Satellite System communication over low-latitude regions
- Equatorial plasma bubbles field-aligned nature and its influence on transionospheric signals aligned with these depleted plasma structures
- Ionospheric scintillation and deep fading characteristics according to the propagation path

Supporting Information:

Supporting Information may be found in the online version of this article.

Correspondence to:

J. Sousasantos,
jonas.ssts@utdallas.edu

Citation:

Sousasantos, J., Affonso, B. J., Moraes, A., Rodrigues, F. S., Abdu, M. A., Salles, L. A., & Vani, B. C. (2022). Amplitude scintillation severity and fading profiles under alignment between GPS propagation paths and equatorial plasma bubbles. *Space Weather*, *20*, e2022SW003243. https://doi.org/10.1029/2022SW003243

Received 31 JUL 2022
Accepted 9 NOV 2022

Abstract Ionospheric scintillation and fading events over low-latitude regions are often caused by severely depleted geomagnetic field-aligned structures known as Equatorial Plasma Bubbles. These events are subject of interest to scientific investigations and concern to technological applications. Over the past several years, most of scintillation studies have focused on the dependence of these events on density gradients, location, local time, geomagnetic conditions, and so forth. This work presents a discussion about the role of the alignment between the signal propagation path and the depleted structures or, equivalently, the geomagnetic field lines, on the observed scintillation and deep fading characteristics. Data from three stations (dip latitudes: 16.13°S, 19.87°S, and 22.05°S) located around the Equatorial Ionization Anomaly (EIA) region were used to assess the amplitude scintillation severity and the deep fading events features under aligned and nonaligned conditions. The results show that the alignment condition plays a crucial role in the occurrence of strong scintillation. The study also revealed that, as stations far from the crests of the EIA are considered, the alignment influence seems to increase, and that a combination of strong plasma density fluctuation and increased aligned path is, presumably, the configuration under which the most severe scintillation and drastic deep fading events are observed. The results indicate that this conjunction is typically met in regions somewhat distinct from that with largest plasma density background over the Brazilian region, therefore, strongest scintillation and largest deep fading rates were observed by a station slightly off-the EIA peak.

Plain Language Summary Several phenomena from space weather affect technological applications dependent on positioning systems relying on information from the Global Navigation Satellite System. Over low-latitude regions the most prominent events are the Equatorial Plasma Bubbles. These plasma bubbles are depleted structures that may reach thousands of km and affect radio signals causing deep fading events and the so-called ionospheric scintillation. Very often the studies regarding plasma bubbles and the ensuing ionospheric scintillation and deep fading events consider the plasma density deviation caused by the presence of these plasma bubbles over a region with enhanced background plasma density, as is the case of the Equatorial Ionization Anomaly, however, this work shows that other aspects must also be considered. In this work scintillation data from ground receivers deployed over the southern Brazilian region during a period of intense occurrence of scintillation were used to uncover new aspects responsible for severe scintillation and deep fading events. It was shown that the alignment between the transionospheric signals and the plasma bubbles is related to the severe scintillation and to the increase in the deep fading events rate. It was also found that the conjoint configuration of strong plasma density deviation and increased alignment is probably responsible for the more drastic events.

1. Introduction

The low-latitude ionospheric phenomenology has strong influence over transionospheric signals such as those used by the Global Navigation Satellite System (GNSS) (Basu et al., 1988; Beach & Kintner, 2001; Kintner et al., 2001). In this dynamic environment, during nighttime, the development of large depletions in the ionospheric plasma density, known as Equatorial Plasma Bubbles (EPBs), may interfere in the satellite links in different ways. There are two major issues of interest regarding GNSS signals over low latitudes, the ionospheric

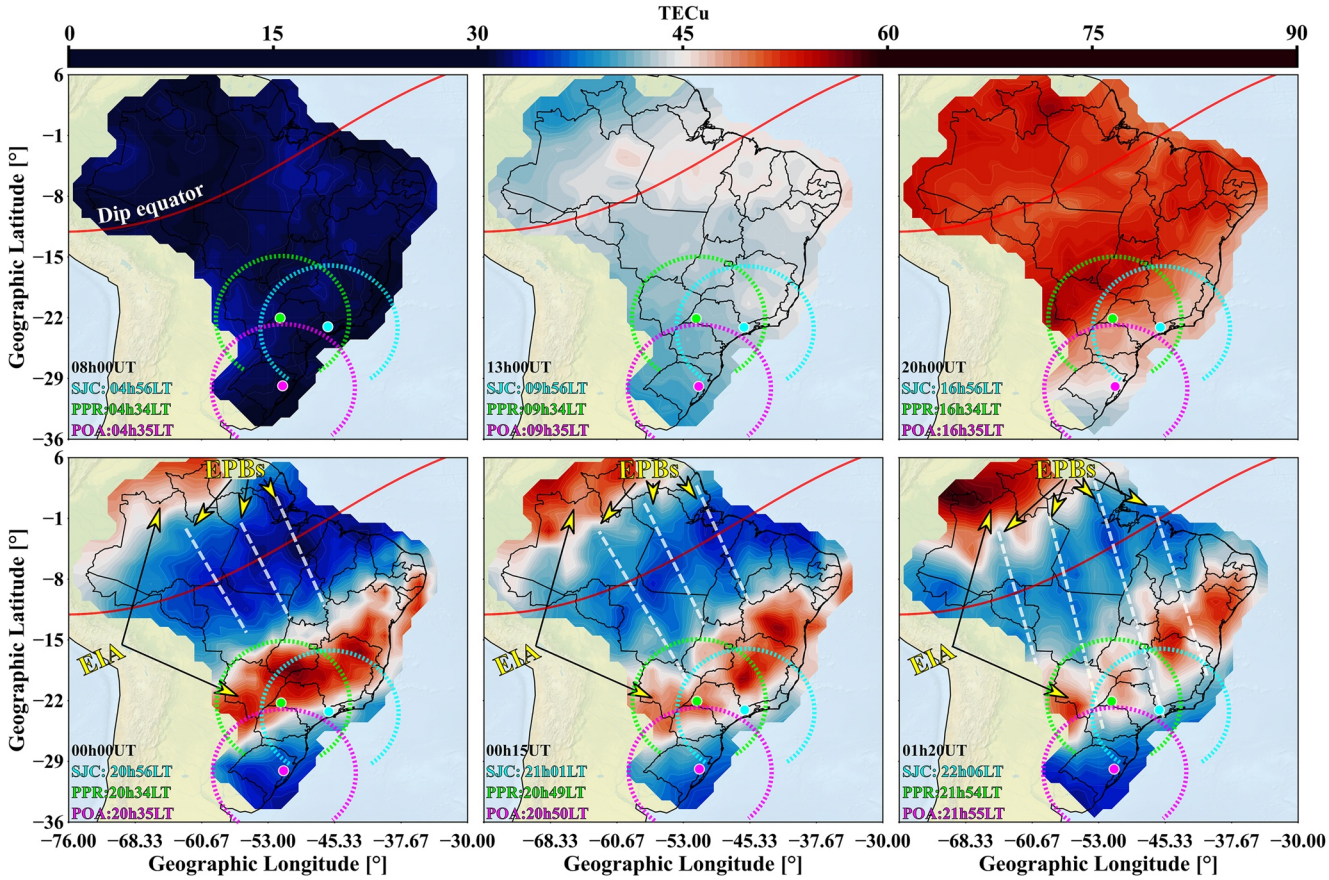

Figure 1. Examples of Total Electron Content (TEC) maps over the Brazilian territory along 11/16/2014. The blue/red colors indicate lesser/larger TEC values, the red line corresponds to the geomagnetic equator, and the white dashed lines denote the regions with signatures of EPBs spreading with time. The dots indicate the location of Presidente Prudente (green), São José dos Campos (cyan) and Porto Alegre (magenta), and the arcs around the stations describe the coverage of the GNSS signals for elevation angles >20°. After 00:00UT, the EPBs start to penetrate progressively into the EIA region causing large gradients of plasma density, that is, sharp spatial fluctuations in the density.

scintillation (Briggs, 1964; Yeh and Liu, 1982) and the fading events, both taking place at the nighttime due to the existence of the EPBs and being capable of degrade and cause temporary outages in GNSS-based systems. Ionospheric scintillation refers to fluctuations in the received signal amplitude and/or phase and is caused by the abrupt variations in the ionospheric index of refraction associated with the EPBs. De Forest (1913) was the first to use the term "fading" to refer to ionospheric interferences in the radio signal transmissions. In this work, fading events are defined as steep and deep decreases estimated from the normalized intensity of the GNSS signal.

The EPB structures causing the ionospheric scintillation and the fading events are believed to be generated over the equatorial region due to the Rayleigh-Taylor instability (Dungey, 1956). These EPB structures develop vertically, and, because of its field-aligned nature, they also propagate along the geomagnetic field toward low-latitude regions. The dimensions of these EPB structures may reach tens of kilometers in the zonal direction and more than 1,000 km in the vertical direction, corresponding to tens of degrees also in latitude. The influence of EPB events is known to be more severe for GNSS users along the Equatorial Ionization Anomaly (EIA) region (e.g., Basu et al., 1988; Beach & Kintner, 2001). This is related to the large plasma concentration and the corresponding enhanced "plasma density deviation" ($\Delta N/N$) (e.g., Briggs & Parkin, 1963).

Figure 1 shows one example of typical EPB events observed over the Brazilian region. In this figure, the Total Electron Content (TEC) is used to evaluate the evolution of the ionosphere under the occurrence of EPBs. The TEC is a measure of the integrated electron density along the ray path considering a cylinder with unitary cross section, and its unity is 10^{16} electrons/m^2. This example shows six panels along 11/16/2014 (mm/dd/yyyy format). The blue/red colors correspond to lesser/larger TEC values according to the color bar above the panels and the red

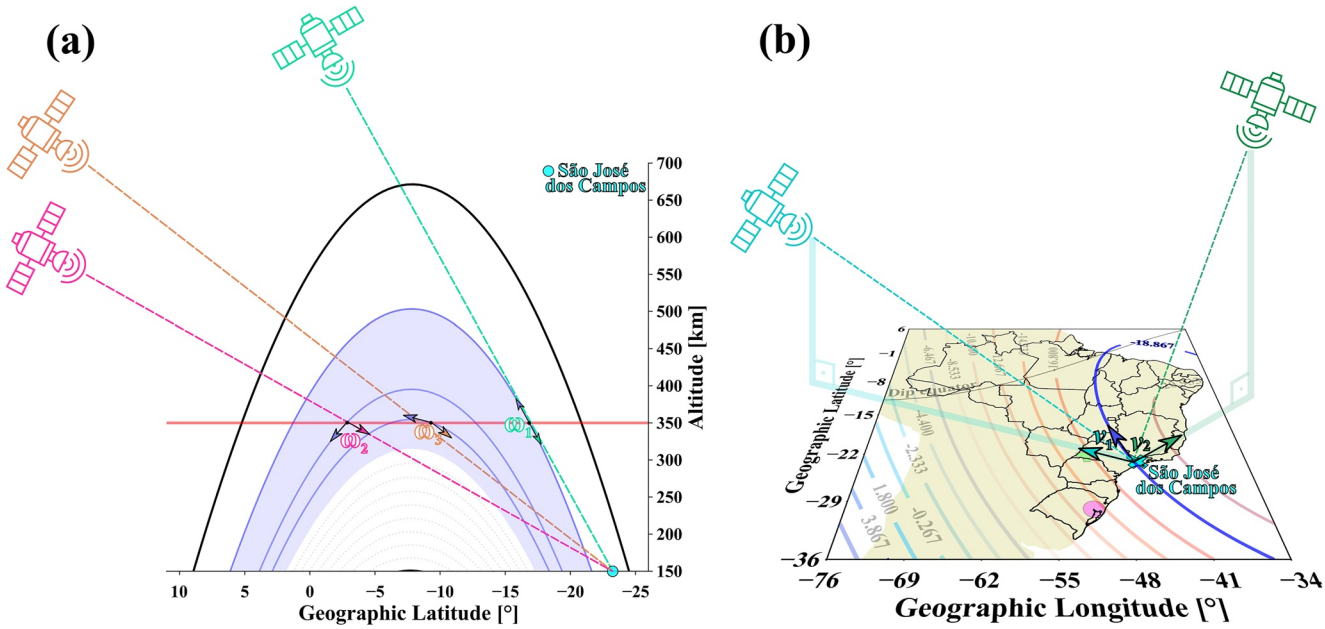

Figure 2. Representation of the alignment between the received signals elevation and azimuth angles and the geomagnetic inclination and declination, respectively. Panel (a): Satellites transmitting to São José dos Campos station under distinct elevation/inclination alignment (ω). Panel (b): Satellites transmitting to São José dos Campos under different azimuth/declination alignment (υ).

line indicates the dip equator. The formation of the EIA (TEC enhancements a few degrees off-the equator) can also be observed in the panels. The dots indicate the locations of Presidente Prudente (PPR) (green), São José dos Campos (SJC) (cyan) and Porto Alegre (POA) (magenta), three GNSS ground stations that will be used along this work. The dashed arcs around each station illustrate the coverage of the GNSS constellation under a condition of elevation angle >20°. White dashed lines denote the EPBs progression path across the TEC map. Please observe that, particularly in this figure, the longitudinal extent of the Brazilian region, from east to west, covers regions with local times corresponding to UT-4.93 up to UT-2.23.

The EPB structures arising at the equatorial region spread to increasingly off-equator latitudes and may reach thousands of km. As mentioned earlier, over the EIA region the level of depletion caused by the EPBs is sharpened due to the larger background plasma density (i.e., larger TEC), therefore, the enhanced plasma density deviation is expected to intensify the scintillation. Please notice that, according to the arcs describing the coverage of the GNSS signals per station, the larger portions of enhanced $\Delta N/N$ take place over PPR, being slightly smaller over SJC and decreasing substantially over POA. An animation of TEC maps showing the evolution of the ionosphere, the EIA location and the EPBs for night of 16–17 November 2014 around the hours depicted in Figure 1 is provided as Supporting Information (Movie S1).

2. Transionospheric Signals and the EPBs Field-Aligned Nature

Briggs and Parkin (1963) and Briggs (1975) proposed that a radio wave trespassing a distance L along an ionized irregular medium suffers more scintillation as larger L are considered, that is, when the signal is more synchronous with the irregular structures. Over low-latitude region, since EPBs are geomagnetic field-aligned structures (Haerendel et al., 1992), this theoretical development from diffraction method indicates that GNSS transmissions with elevation and azimuthal angles more aligned to the geomagnetic inclination and declination, respectively, will experience enhanced scintillation. It is usual to assume a thin-shell model such that the ionospheric density is concentrated and the signal traverses this "shell" at one point referred to as Ionospheric Pierce Point (IPP) (Reilly et al., 1981). Very often, the IPP is assumed at 350 km, and the alignment, therefore, must be considered at this altitude.

Figure 2 illustrates the "alignment condition," depicting how the GNSS elevation and azimuth angles project onto the geomagnetic inclination and declination angles at the IPP altitude. The panel (a) shows a schematic of

the alignment regarding elevation angles and the geomagnetic field inclination. In this pictorial representation, the satellites signals are being received at SJC (out of scale). The red line corresponds to the IPP altitude, and the purple region represents an EPB structure. Each satellite describes a distinct angle of alignment (ω) with the inclination of the geomagnetic field (purple lines).

The panel (b) depicts signals from two satellites being received at SJC. The geomagnetic declination isogonic lines at the IPP altitude were projected onto the map (colored transparent lines), with emphasis on the line over SJC (represented in blue). Each satellite describes a distinct angle (υ) of alignment with the declination of the geomagnetic field line. Since the EPBs follow these geomagnetic field lines, the alignment described by the angles ω and υ indicates the permanence of these GNSS signals across an irregular ionosphere, enhancing the scintillation (increased L).

In a previous study, DasGupta et al. (2004) verified that enhancements in the scintillation were noticed over Calcutta (22.57°N, 88.35°E, dip latitude: 17.35°N), in the Indian sector, when the satellites propagation path was aligned to the geomagnetic field lines. Anderson and Straus (2005), using Global Positioning System (GPS) occultation, found larger values of scintillation when the ray path was aligned to the geomagnetic field. Paul et al. (2011) performed an analysis using dual-frequency GPS receivers deployed at Calcutta during 2008–2010, and also found evidence that the geometry of propagation plays a crucial role in the scintillation strength. Ray et al. (2014) found similar results using 17 receivers from the GPS and Geo Augmented Navigation (GAGAN) network over India. The works by DasGupta et al. (2004), Paul et al. (2011), and Ray et al. (2014) also revealed that the influence of the propagation geometry seems to be enhanced for post-midnight hours, when plasma density and associated irregularities decrease, suggesting a dependence on local time. In addition, Abadi et al. (2014, 2017) found larger values of scintillation for ray paths aligned to the geomagnetic field over the Indonesian region.

Moraes et al. (2017) investigated the effects of the alignment over the Brazilian region assessing each component of the alignment individually. Moraes, Vani, et al. (2018) evaluated how the statistics about scintillation changed according to the alignment of the GPS signals with the plasma bubbles. They showed that, besides stronger scintillation, an increased probability of bit error and, consequently, of cycle slips, was expected under aligned conditions. They also showed that the larger number of cycle slips events degrades more accurate positioning as is the case of the Precise Point Positioning (PPP). The work by Yang and Morton (2020) corroborated the influence of the alignment in the degradation of positioning performance for PPP. Gladek et al. (2019) and Vani et al. (2021) suggested that changes in the fading profiles are related to aligned condition. Saito et al. (2009) and Yoon et al. (2020) also reported consequences of the alignment in spatial decorrelation. Complementing these works, Affonso et al. (2022) analyzed in detail the alignment condition and showed that, over low-latitude regions, this is a source of strong ionospheric gradients. However, several aspects remain uncovered and requiring further investigation. These aspects will be discussed in this work and include: (a) How the severity of the amplitude scintillation is related to the alignment condition over the Brazilian region? (b) How strong is the alignment influence considering ground stations in distinct locations around the EIA? (c) Is there any relation between the larger occurrence of scintillation and the more severe scintillation, that is, the station with a greater number of cases is that suffering the more drastic scintillation? (d) Where the configuration that leads to the more severe scintillation cases were experienced over the Brazilian region more often? (f) What is the influence of the alignment on deep fading events? More specifically, does the alignment cause increases in the number of deep fading events?

3. Instruments and Methods

Ionospheric amplitude scintillation observations analyzed in this study were made by Septentrio PolaRxS PRO scintillation monitors (Sreeja et al., 2011), which are part of the CIGALA/CALIBRA network (Monico et al., 2013). These are state-of-the-art GNSS multi-constellation, multi-frequency sensors for monitoring ionospheric scintillation and TEC. For this study, the measurements of the GPS L1 signal (1,575.42 MHz) were used. Additionally, to mitigate the effects of multipath on the measurements, only satellites with elevation higher than 20° were considered.

The analyses focused on solar maximum conditions during the period between 01 November 2014 and 31 March 2015 for time intervals ranging from 19:00 LT up to 24:00 LT. These are months and hours when EPBs and

Table 1
Information About Station Locations, Number of Observations (Records) and Number of Aligned/Nonaligned Scintillation Cases

	Presidente prudente (PPR)	São José dos Campos (SJC)	Porto alegre (POA)
Geographic Latitude [°]	−22.12	−23.20	−30.07
Geographic Longitude [°]	−51.40	−45.85	−51.11
Geomagnetic Inclination [°]	−30.01	−35.82	−38.98
Geomagnetic Declination [°]	−16.97	−19.41	−14.74
Dip latitude [°]	−16.13	−19.87	−22.05
Local Time	UT-3.43	UT-3.06	UT-3.41
Total number of records (with or without scintillation)	252,934	264,682	233,582
Nonaligned cases ($S_4 > 0.25$)	53,069	32,907	8,268
Aligned cases ($S_4 > 0.25$)	4,385	4,001	2,064
Percentage of scintillation cases	22.71%	13.94%	4.42%

L-band scintillation are known to occur frequently in the Brazilian sector where the scintillation monitors available to this study were installed (Sobral et al., 2002; Sousasantos et al., 2018).

To evaluate the severity of amplitude scintillation we used the S_4 index which can be defined as (Ryle & Hewish, 1950; Yeh and Liu, 1982):

$$S_4 = \left[\frac{\langle I^2 \rangle - \langle I \rangle^2}{\langle I \rangle^2} \right]^{1/2}, \quad (1)$$

where I corresponds to the intensity of the received signal and the $< >$ brackets indicate average values calculated over a given time interval. In this work, the S_4 index was computed using samples measured at 50 Hz sampling rates for intervals of 60 s. The S_4 is a measure of the root mean square deviation of the intensity from its mean value, normalized by the mean intensity along the interval (Briggs, 1975).

Table 1 provides information about the location and local time of the scintillation monitors, observations available (with or without scintillation), and the number of aligned/nonaligned scintillation cases per station considering $S_4 > 0.25$. Note that the locations of the stations are also depicted in Figure 1. The largest percentages of scintillation occurrences ($S_4 > 0.25$ aligned and nonaligned cases) were registered by the PPR station, being followed by SJC, and POA.

The alignment condition for each S_4 measurement was also evaluated. First, the mean IPP coordinates for each 60 s of record were calculated. Subsequently, the geomagnetic field inclination and declination angles were obtained from the International Geomagnetic Reference Field (IGRF-12) (Thébault et al., 2015) for each of the IPP coordinates. Next, the angles of alignment (ω and ν) were calculated (Moraes, Vani, et al., 2018). As mentioned earlier, ω corresponds to the angle difference between the propagation path elevation and the geomagnetic inclination, as illustrated in the panel (a) of Figure 2, and ν represents the angle difference between the propagation path azimuth and the geomagnetic declination, as shown in the panel (b) of Figure 2. In this work, an observation was said to be "under aligned condition" when both $|\omega|$ and $|\nu|$ are $\leq 15°$. As one example, let the SJC station and the elevation angle at its IPP to be considered. Since the inclination of the geomagnetic field lines changes smoothly in the regions around the plasma density peak (e.g., inclination = −35.87° at 350 km and inclination = −35.09° at 600 km), if $\omega \leq 15°$, this means that the ray path at 600 km is distant by, at most ~33 km of the field line. If the declination is considered instead, the numbers are very similar. Please observe that EPBs may reach hundreds of kilometers (e.g., Huang et al., 2012), therefore, angles ≤15° may be assumed with no loss of generality.

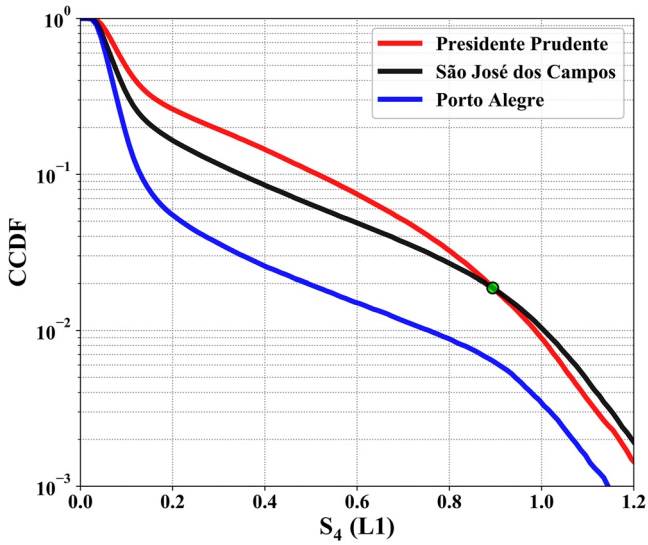

Figure 3. Complementary Cumulative Distribution Function (CCDF) of S_4 for all the stations considered.

4. Results and Discussion

To introduce the discussion, a summary of the results through Complementary Cumulative Distribution Functions (CCDF) of the S_4 values measured by the three stations considered in this work is presented. Previous studies such as Moraes, Muella, et al. (2018) (Figure 4 in their paper) and Salles, Vani et al. (2021) (Figure 7 in their paper) used the CCDF to quantify scintillation occurrence according to the S_4 levels and the variability of the occurrence with location, signal frequency and season.

Figure 3 shows that the occurrence of weak to strong scintillation events ($0.2 < S_4 < 0.9$) is higher for PPR (red) than what is observed in SJC (black) and POA (blue). For instance, scintillation events with $S_4 > 0.5$ show an occurrence rate of 10% (i.e., $P(S_4 > 0.5) = 0.1$) for PPR, 6% for SJC and 2% for POA. The differences in scintillation occurrences may be explained, at least in part, by the fact that the IPPs of the signals measured in PPR are mostly contained in the EIA region, where density perturbations with larger amplitudes (larger ΔN) are expected to occur. Please observe that the percentages in Table 1 already suggested this result.

According to Figure 3, when severe scintillation ($S_4 > 0.9$) cases are considered, the CCDF reveals highest rates observed by the SJC station. This transition ($S_4 \sim 0.9$) is indicated by a green dot in Figure 3. For instance, for $S_4 > 1.0$ probabilities around 0.8%, 1%, and 0.3% for PPR, SJC, and POA, respectively. This result indicates that factors other than the location of the station must also control scintillation strength severity.

4.1. On the Effects of Alignment on Amplitude Scintillation Severity

The results in Figure 3 are related to the effects of the variations in the amplitude of density perturbations (ΔN) and in the thickness of the irregularity layer (L) traversed by the signals. The severity of amplitude scintillation is proportional to L and to ΔN (Basu et al., 1976; Briggs & Parkin, 1963; Rino, 1979a, 1979b). Larger ΔN irregularities are expected to occur in regions of larger background ionospheric density. This is the usual explanation for the observation of intense scintillation near the EIA region. Additionally, when signals are aligned with the geomagnetic field, they are more likely to pass through a broader (thicker, larger L) region of irregularities due to the field-aligned nature of EPBs.

Considering the ground stations chosen for this work, PPR is located near the center of the southern EIA crest in Brazil, as a result, signals measured by this station often traverse the EIA crest and experience the effects of large ΔN, suffering intense scintillation. SJC, on the other hand, is located poleward of the southern EIA crest. The signals measured by SJC do not pass through large ΔN as frequently as those observed by PPR. As a result, intense scintillation over SJC requires an increased contribution of large L, that is alignment, when compared to PPR. The same is true for POA, which is located well outside of the EIA crest. Intense scintillation over POA is even more dependent of large L (alignment) conditions.

Figure 4 serves to support the considerations aforementioned and shows the percentages of occurrence of scintillation under alignment (red) and nonalignment (blue) conditions for the three stations. More importantly, these percentages are exhibited according to the corresponding S_4 values. Each bin contains the occurrences of the respective $S_4 \pm 0.05$, therefore corresponding to $0.25 \leq S_4 \leq 1.25$. The panels reveal that, as increasing values of amplitude scintillation are considered, the percentages of aligned cases grow for all stations as well.

The upper panel shows the results over PPR and indicates that, for $S_4 \geq 1$, the aligned cases correspond to 25.90%, 30.67%, and 39.42%, respectively. Please observe that PPR is located in the EIA crest and signals received at this station frequently propagate through regions of large ΔN. Figure 4 also shows that the contribution from the alignment conditions to intense scintillation increases in SJC (middle panel) compared to PPR. For $S_4 \geq 1$, the aligned cases correspond to 36.32%, 40.02%, and 45.96%, respectively. This is because SJC is located outside the EIA crest. Less cases of large ΔN are occurring and alignment (large L) is required for intense scintillation

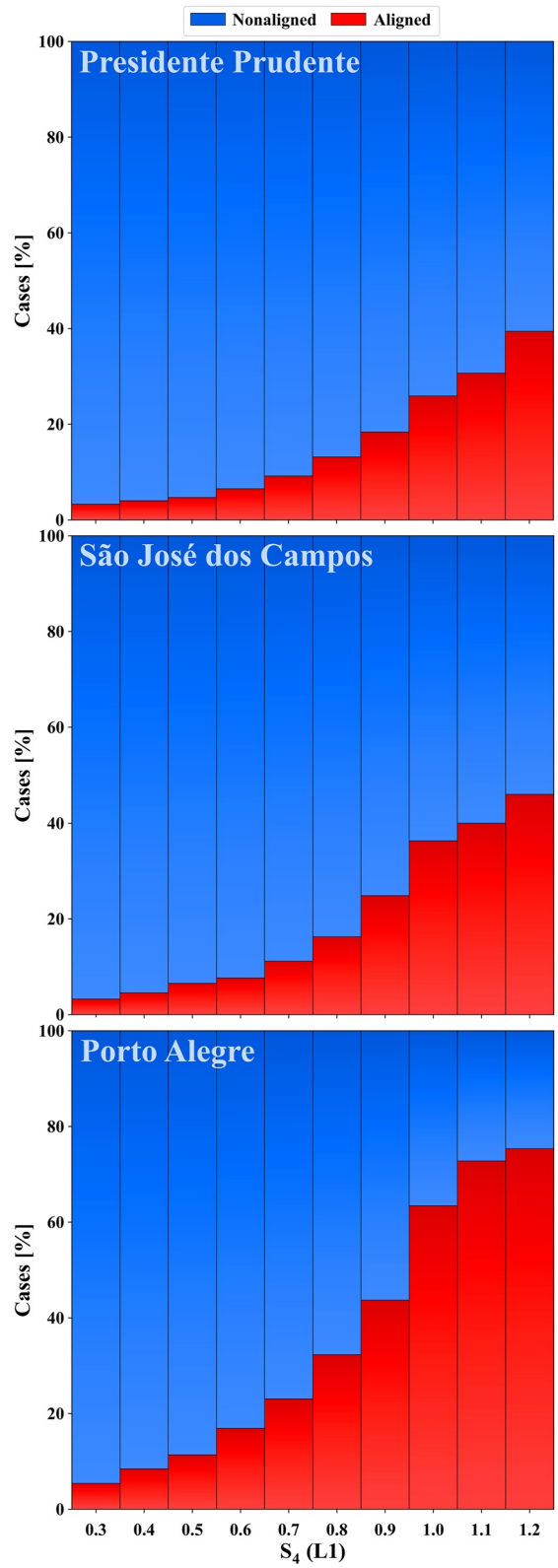

Figure 4. Percentages of aligned (red) and nonaligned (blue) cases according to the S_4 values for the stations of Presidente Prudente (upper panel), São José dos Campos (middle panel) and Porto Alegre (lower panel). The results indicate that cases of strong scintillation seem to be influenced by the aligned propagation orientation.

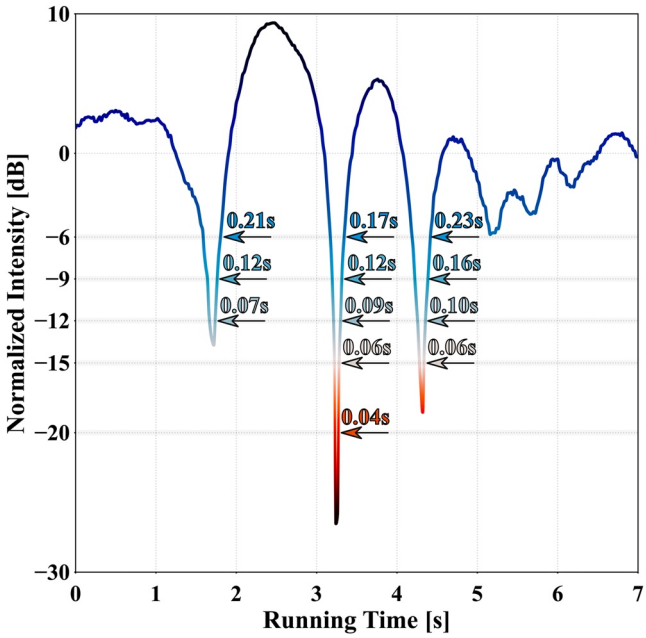

Figure 5. Example of fading events with signal intensity dropping to levels below the thresholds of −6, −9, −12, −15, −20 dB. The durations of these events are also informed.

to be observed. Finally, intense scintillation in POA (lower panel) occurs, predominantly, when signals meet the alignment condition being, for $S_4 \geq 1$, 63.45%, 72.78%, and 75.35%, respectively. This is because POA is even more outside of the EIA than SJC. The signals observed at POA are expected to experience mostly weak density perturbations (smaller ΔN cases). In that scenario, alignment (large L) is also required for intense scintillation to be observed. These results indicate that severe scintillation over stations progressively away from the EIA region presents an increasing dependence on the alignment condition.

One of the most interesting aspects of these results is that, for the region considered, most of the time the satellites paths are not aligned with the geomagnetic field, and observations under the condition of alignment are only a small fraction of the total number of the observed scintillation cases. According to Table 1, the percentage of aligned observations for PPR, SJC, and POA were 7.63%, 10.84%, and 19.98%, respectively. Despite this smaller number of aligned observations, these cases corresponded to almost half of the severe scintillation over SJC and even more over POA.

In addition, is worth notice that, although PPR is the station with the larger coverage of IPPs around the EIA region (e.g., see Figure 1), due to the geometry of the geomagnetic field and the trajectories of the GPS satellites, the alignment condition is typically met around the northern boundary of the southern EIA crest. Consequently, when L increases ΔN is not at its maximum. For SJC the alignment condition is generally met closer to the center of the southern EIA crest, hence, regardless of a slightly small intersection between its IPPs coverage and the EIA, the larger L is found to be coincident with maximized ΔN, therefore, worsening the scintillation severity. This is, probably, the reason for the highest rates of observed $S_4 > 0.9$ (i.e., severe scintillation) for SJC instead of PPR in Figure 3. For POA the intersection between the IPPs coverage and the EIA is the smallest and the alignment is met at the southern boundary of the southern EIA crest. Please observe that, although the EIA location may vary (e.g., Balan et al., 2018), the overall average EIA peak location during the period of analysis (Li et al., 2018) supports the arguments discussed in this manuscript.

4.2. On the Effects of Alignment on Fading Occurrence Rates and Duration

In this section the results related to the analysis of the number of fading events per minute and average duration of the observed fading events (in seconds) are presented. Fading events are defined as steep and deep decreases estimated from the normalized intensity of the GPS signal.

The average time duration and the number of fading events recorded during each minute, for each of the three stations, were computed considering five thresholds of fading levels used to classify the events: −6, −9, −12, −15, and −20 dB.

Figure 5 shows one example of fading events using 7 s of GPS L1 intensity data from satellite PRN 25 (PRN stands for Pseudo Random Noise) recorded by the SJC monitor on 13 November 2014. Intensity data was detrended and normalized. Each arrow color corresponds to one of the fading level thresholds. The colors from blue to red indicate gradually deeper fading events. For each fading event detected, the duration (in seconds) is also informed to the right of the fading "bite-outs."

The left panels of Figure 6 summarize the results related to fading event occurrence rates for the measurements made in PPR (upper left panel), SJC (middle left panel), and POA (lower left panel). For each station, for each value of $S_4 \pm 0.05$ with $S_4 \in \{0.3, 0.4, 0.5, 0.6, 0.7, 0.8, 0.9, 1.0, 1.1, 1.2\}$, the fading events deeper than a given fading threshold (i.e., −6, −9, −12, −15, −20 dB) for each 60 s interval were grouped. After the grouping process along the entire data set these events were properly summed and divided by the total number of occurrences of the respective group of values of $S_4 \pm 0.05$. This procedure was performed for each of the fading thresholds (distinguished by the colors) and for aligned (solid lines) and nonaligned (dashed lines) cases, individually.

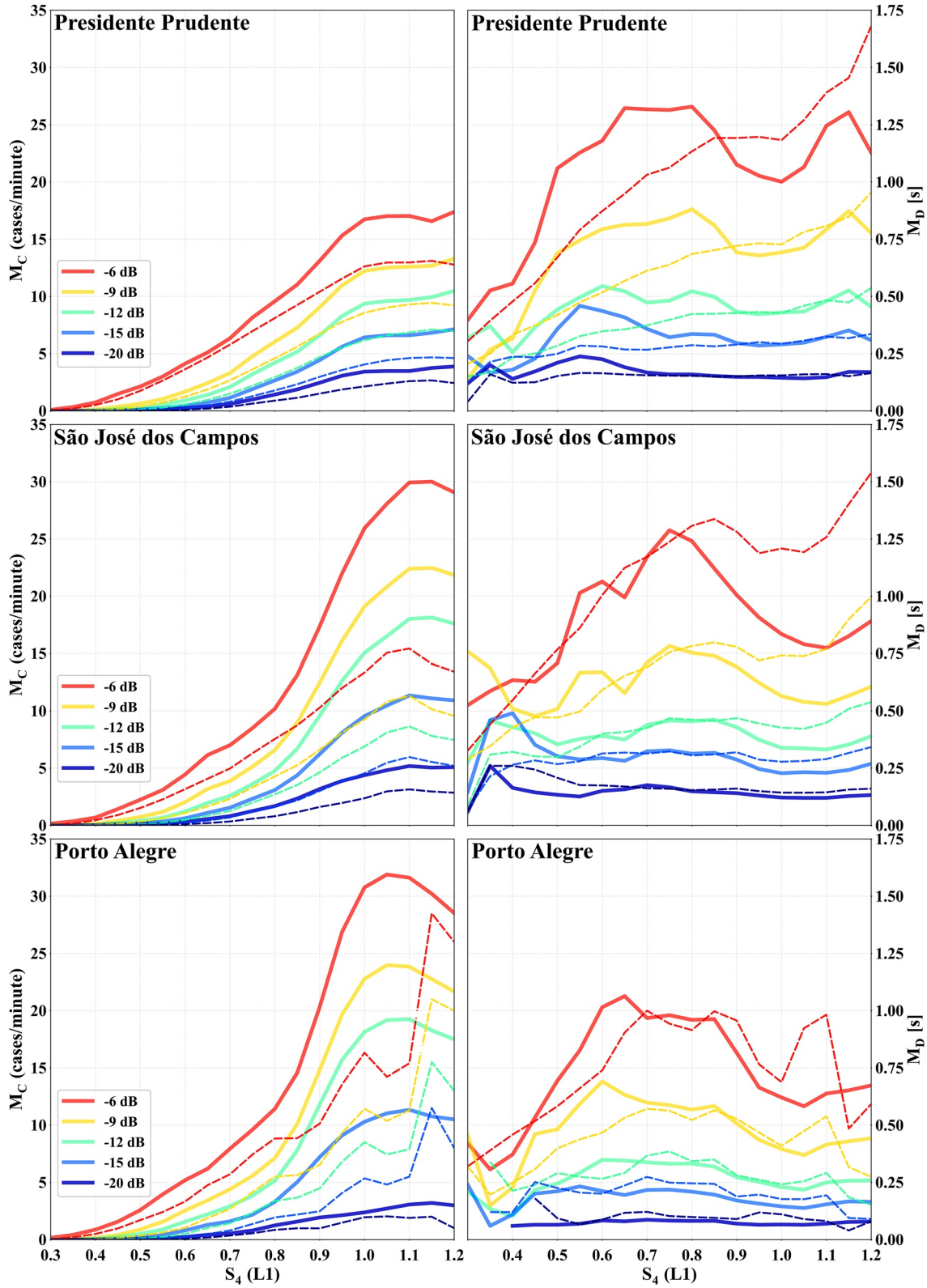

Figure 6. Average number of fading occurrences per minute (left) and duration of fading events (right) according to the S_4 levels estimated for the aligned (solid lines) and nonaligned (dashed lines) received signals. The upper/middle/lower panels show the results for Presidente Prudente/São José dos Campos/Porto Alegre stations, respectively. The colors indicate each of the thresholds of fading depth levels evaluated.

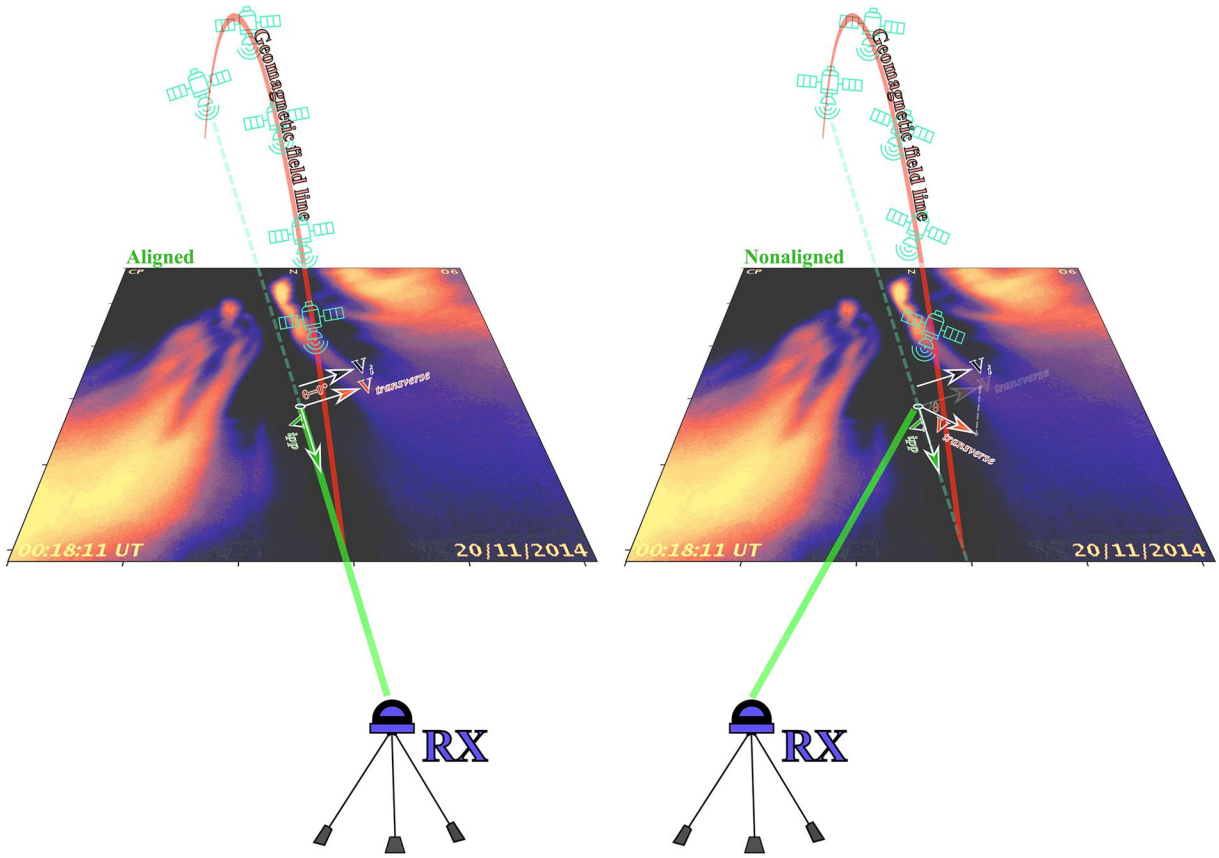

Figure 7. Pictorial sketch of the geometry of irregular diffracting structures (EPBs) speed in relation to the satellite-receiver propagation path explaining fading rates/rapidity. Left panel: The ray path (green solid line) is aligned with the structure, $V_{\text{transverse}}$ is maximized, and the fading rates increase. Right panel: The ray path is not aligned and the $V_{\text{transverse}}$ is smaller, therefore decreasing the fading rates and increasing the duration of the events for a given signal path.

These panels serve to quantify the number of fading events per minute (M_C) one can expect for different S_4 values and for stations located at low latitudes and near the EIA. The first aspect revealed is that M_C, for any fading depth, increases with S_4 until about $S_4 = 1.0$. However, the most interesting result in the left panels of Figure 6 is that, regardless of the S_4 range, fading threshold, or station, the fading rates for aligned cases are always larger than the rates for the nonaligned cases. This is more evident for moderate and intense scintillation events.

A possible explanation is related to the EPB motion (Sousasantos et al., 2021). It is reasonable to expect that the number of fading events observed in 1 minute of records will be controlled by how fast the diffracting structure (irregularity layer) moves across the satellite-receiver signal path or vice-versa. Here, we remind the reader that EPBs are aligned with the geomagnetic field lines and move in the magnetic zonal direction. Therefore, the speed of the diffracting structure is regulated by the component of the irregularity velocity relative to IPP that is transverse to both, the geomagnetic field and signal path ($V_{\text{transverse}}$). Since the IPPs of the GPS signals move mostly in the north-south direction, the occurrence of larger values of $V_{\text{transverse}}$ maximizes when signal path is aligned with the geomagnetic field lines.

Figure 7 presents a sketch of this configuration, the left/right panels correspond to the aligned/nonaligned cases. An EPB optical record from an all-sky imager deployed close to SJC is used as a visual reference. The EPB is the dark streak in the north-south direction crossing the EIA, represented by the brighter region. In the left panel, the GPS-receiver signal path (solid green line) is aligned with the EPB structure so that $V_{\text{transverse}}$ is maximized and the EPB structures will cross the signal path more frequently, or equivalently, more EPBs must cross the ray path. In the right panel, the GPS-receiver signal path (solid green line) is not aligned with the EPB; hence, the diffracting structure remains more time in the ray path decreasing the fading rates. This suggested description would also indicate that shorter duration fading events are more likely to occur during alignment conditions.

Back to Figure 6, the right panels exhibit the results regarding the duration of the observed fading events for PPR (upper right panel), SJC (middle right panel) and POA (lower right panel). For each station, for each value of $S_4 \pm 0.05$ with $S_4 \in \{0.3, 0.4, 0.5, 0.6, 0.7, 0.8, 0.9, 1.0, 1.1, 1.2\}$, the duration of the fading events deeper than a given fading threshold (i.e., −6, −9, −12, −15, −20 dB) for each 60 s interval were averaged. After the averaging process along the entire data set these events were properly summed and divided by the total number of occurrences of the respective group of values of $S_4 \pm 0.05$. This procedure was performed for each of the fading thresholds (distinguished by the colors) and for aligned (solid lines) and nonaligned (dashed lines) cases, individually.

The results indicate that scintillation occurring under alignment conditions are, on average, more likely to produce faster fading events in cases with large amplitude scintillation, conditions under which is more difficult to track the data properly (Humphreys et al., 2010; Portella et al., 2021).

4.3. On the Convergence of Severe Scintillation and Deep Fading Events Along the Geomagnetic Field Lines

To provide a broader view of the results presented so far, Figures 8 and 9 were produced. In Figure 8 the entire S_4 data set were depicted for the stations of PPR (upper panels), SJC (middle panels), and POA (lower panels). Each value of S_4 is displayed at the corresponding IPP location. The nonaligned/aligned cases were exhibited in the left/right panels. The color bar at the right describes the levels of the amplitude scintillation. The ground stations of PPR, SJC and POA are represented by green, cyan, and magenta dots, respectively. Black lines depict the isogonic lines of the geomagnetic field (i.e., declination isolines) at the IPP altitudes. Thicker and dashed graphical representation was employed to emphasize declination lines more coincident with the ground stations. As may be clearly noticed along the panels of this figure, PPR presents the largest amount of scintillation events, followed by SJC and finally POA. Notwithstanding, the aligned cases seem to be consistently more concentric with the field lines and more conterminous with the EIA for the SJC stations. In any case, the concentrations of the severe scintillation for all the stations were found to be always aligned to the geomagnetic field lines.

Figure 9 is similar to the previous, however, it presents the summation of cases of deep fading events (<-15 dB) per minute. All the graphical elements and disposition of the panels are analogous to those before, with the color bar, this time, describing the number of deep fading events per minute, that is, the rate of deep fading events. The rate of deep fading events is reasonably comparable over PPR (upper panels) and SJC (middle panel), being larger for this last. Over POA, the deep fading events rate is, in general, smaller, and revealing less variance. The matter of interest for the present work is the fact that the rates of deep fading events are narrowly confined to the geomagnetic field line direction. Outside the "alignment region" the rate decays steeply for all the stations. It is also true that as the deviation from the EIA increases (corresponding to a decrease of ΔN) the rate also presents an accentuate decrease, hence, ΔN and L again seem to influence conjointly the fading events profiles. Regarding the temporal occurrence of the aligned cases with $S_4 > 0.25$, the concentration of cases is typically around the intervals of 20:00–22:30 LT, 20:00–23:30 LT, and 20:20–22:00 LT for PPR, SJC, and POA, respectively, decreasing for later hours (see Figure S1 in Supporting Information S1).

The same results presented in Figures 8 and 9 were depicted using a sky-plot representation (i.e., azimuth and elevation polar plot) and are available as Supporting Information S1 (Figure S2). The intervals of azimuth and elevation aligned for each ground station may be consulted in this Supporting Information S1 file.

Although this work was focused on GPS L1 data, Salles, Vani et al. (2021) and Salles, Moraes et al. (2021) showed that L2C and L5 are more degraded than the L1 carrier, hence, it is expected that the alignment condition will prejudice even more the availability of these optional frequencies. In addition, it is true that dual frequency approach may be effective to monitor ionospheric gradients (Felux et al., 2017), notwithstanding, when alignment condition occurs, the eventual loss of receiver lock may cause the loss of the observables and the consequent impossibility of gradient estimation. This is especially critical since the propagation path of both frequencies to be considered are aligned.

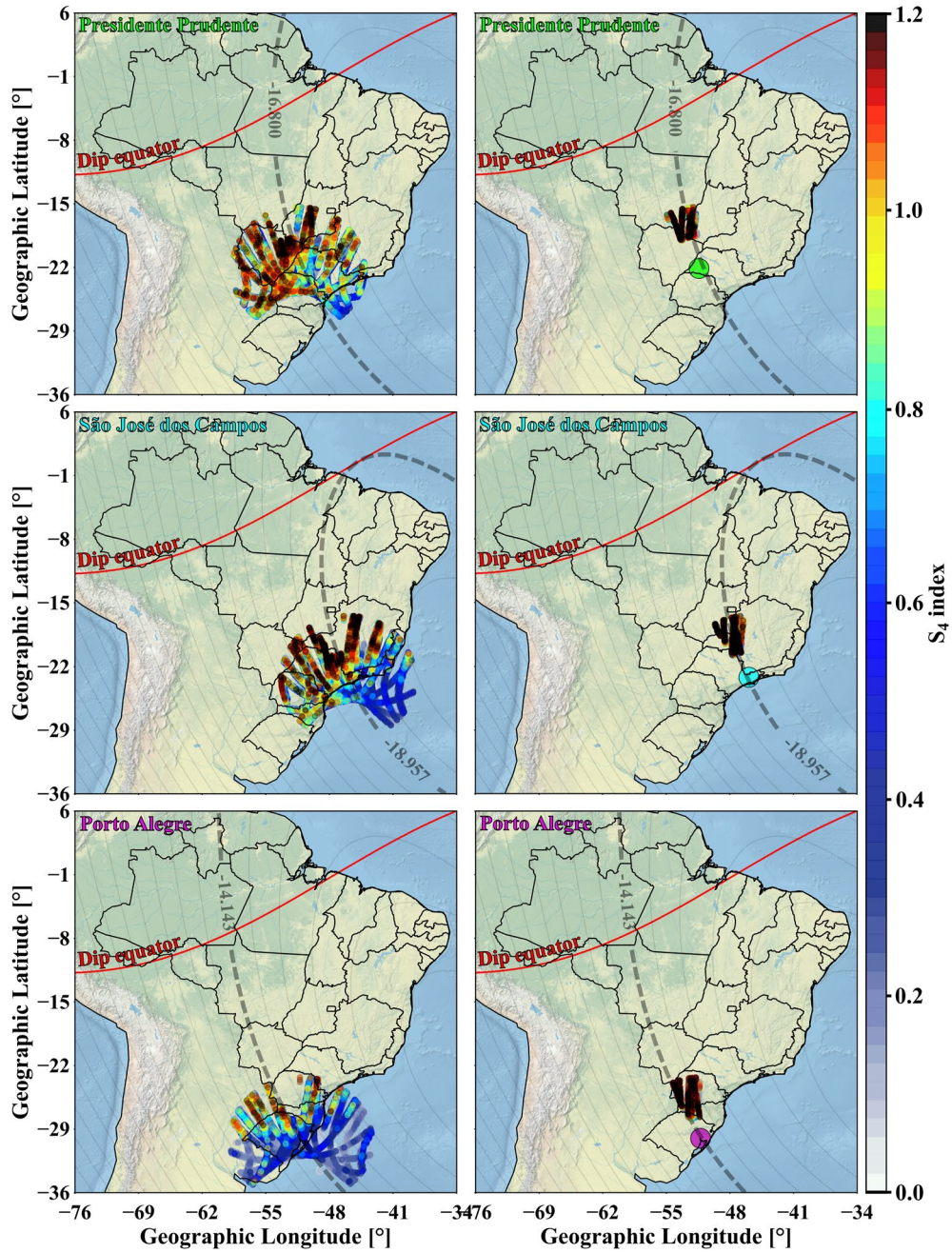

Figure 8. Amplitude scintillation (colors) at corresponding IPP locations for the entire data set. The left panels present all the nonaligned records for Presidente Prudente (green dot, upper panels), São José dos Campos (cyan dot, middle panels) and Porto Alegre (magenta dot, lower panels). The right panels display only the aligned cases for these stations. Isogonics are also depicted by black lines.

5. Concluding Remarks

Several studies about the ionospheric scintillation occurrences over distinct regions proposed explanations that are mostly related to the plasma density fluctuation ($\Delta N/N$) that is crossed by the GPS signals. Nevertheless, the present work shows that some other aspects must also be considered, especially for severe scintillation events. The alignment of radio waves, such as those from the GPS signals, with the geomagnetic field is a crucial parameter when EPB diffracting patterns are occurring at the signal path. Since the EPBs are field-aligned depleted structures, the alignment with the geomagnetic field implies an alignment with the EPBs as well. The

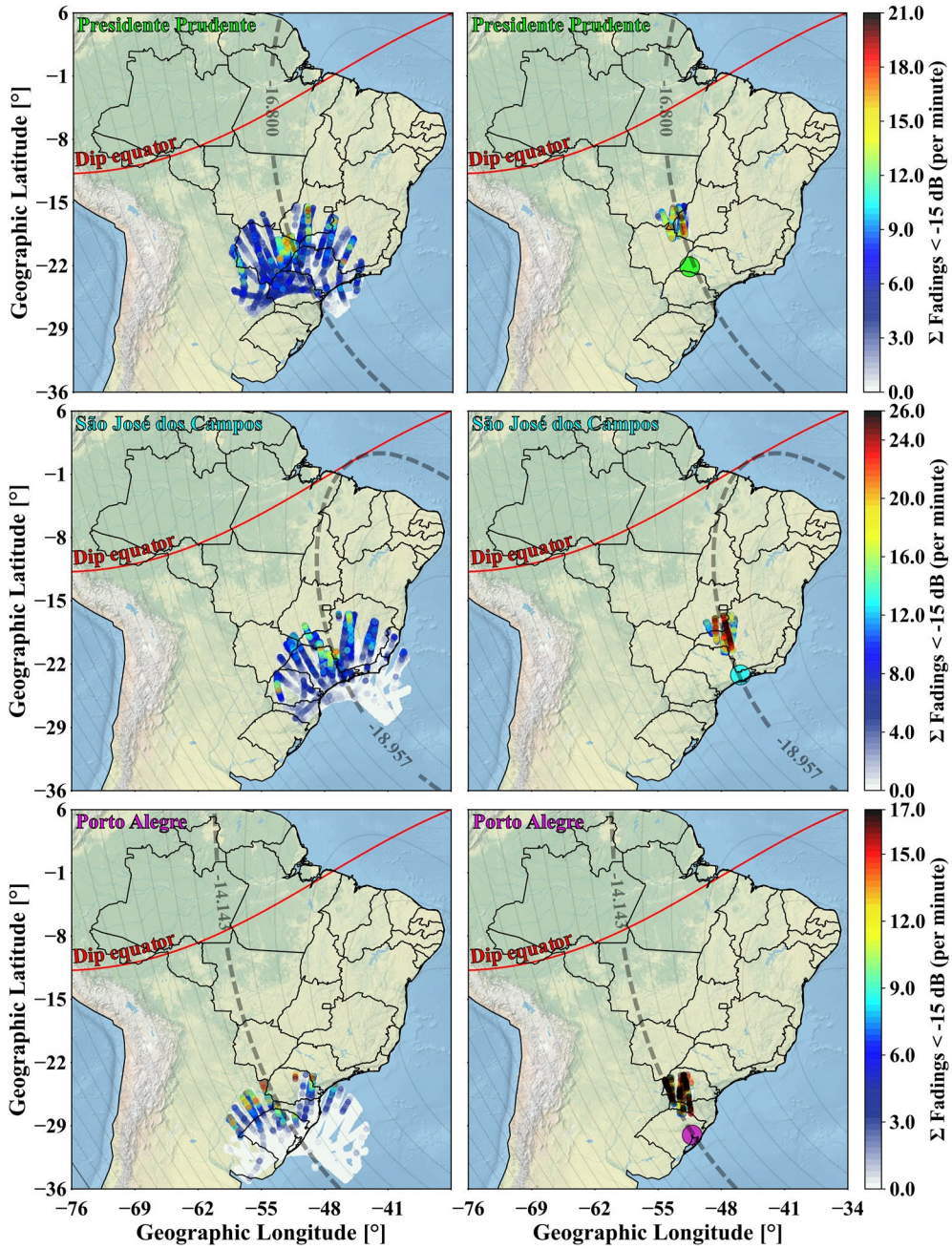

Figure 9. Rate of deep (<−15 dB) fading events (colors) at corresponding IPP locations for the entire data set. The left panels present all the nonaligned records for Presidente Prudente (green dot, upper panels), São José dos Campos (cyan dot, middle panels) and Porto Alegre (magenta dot, lower panels). The right panels display only the aligned cases for these stations. Isogonics are also depicted by black lines. The confinement of the rates along the geomagnetic field line direction is noticeable.

referred alignment is considered at the IPP altitude (i.e., 350 km), and consists of coincidences between the signal elevation/azimuth angles with the geomagnetic inclination/declination, respectively. When a signal presents both components aligned (meaning angle differences <15° in this work), the signal traverses a larger path (L) inside the density fluctuation region. Data from three GPS (L1) receiver ground stations along the Brazilian territory were used to cover the region of larger plasma density concentration (EIA) and its nearness. Data covers 01 November 2014–31 March 2015 from 19:00 LT up to 24:00 LT.

The aspects evaluated in this work include rate of scintillation occurrence and deep fading characteristics under aligned and nonaligned conditions. The main findings may be summarized as follows:

1. The alignment condition role seems to be more noticeable for strong scintillation events ($S_4 > 0.7$).
2. The alignment condition influence increases as stations more off-the-EIA (poleward) are considered. Probably the decreased ($\Delta N/N$) requires an increased L to support the EPB diffractive interference.
3. The coverage of the PPR station IPPs encompasses the largest portion of the EIA, and the station experiences the greatest number of scintillation occurrence. However, the more severe scintillation events were observed by the SJC station, which is slightly away from the EIA crest region.
4. The results indicate that a conjunction of larger $\Delta N/N$ and L is more likely to be the configuration under which severe scintillation occurs over low latitudes. Please notice that the alignment conditions for PPR, SJC, and POA are met, respectively, at the northern boundary, middle and southern boundary of the EIA southern crest, therefore, SJC experience a region of large $\Delta N/N$ and increased L.
5. The number of deep fading events per minute is larger during aligned conditions, meaning faster fading rate and more problems expected in the receiver loops. The average duration of the deep fading events (<-15 dB) also presents some correspondence with the increased alignment influence.

The analyses in this work unveil new relevant aspects regarding the alignment condition influences on signal degradation. These aspects include the dependence of severe scintillation on aligned condition, the combination of larger density fluctuations ($\Delta N/N$) with increased L, and the deep fading rates under aligned conditions. Consequently, when analyzing data from GPS signals one must not only consider the density fluctuation influence as usual, but also the alignment with the geomagnetic field line and the region where both are maximized.

Data Availability Statement

GPS data was provided by the Instituto Brasileiro de Geografia e Estatística (IBGE) under the Rede Brasileira de Monitoramento Contínuo (RBMC) (https://www.ibge.gov.br/en/geosciences/geodetic-positioning/geodetic-networks/20079-brazilian-network-for-continuous-monitoring-gnss-systems.html?=%26t=downloads). All-sky data was provided by the Estudo e Monitoramento Brasileiro do Clima Espacial (EMBRACE) portal (http://www2.inpe.br/climaespacial/portal/en/). The scintillation data used in this paper is available to download through the CIGALA/CALIRA website: http://is-cigala-calibra.fct.unesp.br/is/index.php.

Acknowledgments

J. Sousasantos acknowledges NSF award AGS-1916055 and FAPESP award 2018/06158-9. A. O. Moraes is grateful to CNPq (309389/2021-6). F. S. Rodrigues acknowledges NSF awards AGS-1916055 and AGS-2122639. M. A. Abdu is grateful to the support received from the São Paulo State Foundation for Promotion of Research (FAPESP) through the Process 2016/24970-7. L. A. Salles acknowledges CAPES for financial support under process 88887.495093/2020-00. B. C. Vani thanks INCT GNSS-NavAer, funded by CNPq (465648/2014-2), FAPESP (2017/50115-0), and CAPES (88887.137186/2017-00). Authors would like to thank the International Association of Geomagnetism and Aeronomy (IAGA) and all the scientific and technical staff responsible for the distribution of the International Geomagnetic Reference Field (IGRF). Projects CIGALA/CALIBRA were funded by the European Commission (EC) in the framework of awards FP7-GALILEO-2009-GSA and FP7–GALILEO–2011–GSA–1a, as well of FAPESP award 06/04008-2.

References

Abadi, P., Otsuka, Y., Shiokawa, K., Husin, A., Liu, H., & Saito, S. (2017). Equinoctial asymmetry in the zonal distribution of scintillation as observed by GPS receivers in Indonesia. *Journal of Geophysical Research: Space Physics*, *122*(8), 8947–8958. https://doi.org/10.1002/2017JA024146

Abadi, P., Saito, S., & Srigutomo, W. (2014). Low-latitude scintillation occurrences around the equatorial anomaly crest over Indonesia. *Annales Geophysicae*, *32*(1), 7–17. https://doi.org/10.5194/angeo-32-7-2014

Affonso, B. J., Moraes, A. O., Sousasantos, J., Marini-Pereira, L., & Pullen, S. (2022). Strong ionospheric spatial gradient events induced by signal propagation paths aligned with equatorial plasma bubbles. *IEEE Transactions on Aerospace and Electronic Systems*, *58*(4), 2868–2879. https://doi.org/10.1109/TAES.2022.3144622

Anderson, P. C., & Straus, P. R. (2005). Magnetic field orientation control of GPS occultation observations of equatorial scintillation. *Geophysical Research Letters*, *32*(21), 1–4. https://doi.org/10.1029/2005GL023781

Balan, N., Liu, L., & Le, H. (2018). A brief review of equatorial ionization anomaly and ionospheric irregularities. *Earth and Planetary Physics*, *2*(4), 257–275. https://doi.org/10.26464/epp2018025

Basu, S., Basu, S., & Khan, B. K. (1976). Model of equatorial scintillations from in-situ measurements. *Radio Science*, *11*(10), 821–832. https://doi.org/10.1029/RS011i010p00821

Basu, S., MacKenzie, E., & Basu, S. (1988). Ionospheric constraints on VHF/UHF communications links during solar maximum and minimum periods. *Radio Science*, *23*(3), 363–378. https://doi.org/10.1029/RS023i003p00363

Beach, T., & Kintner, P. M. (2001). Development and use of a GPS ionospheric scintillation monitor. *IEEE Transactions on Geoscience and Remote Sensing*, *39*(5), 918–928. https://doi.org/10.1109/36.921409

Briggs, B. H. (1964). Observations of radio star scintillations and spread-F echoes over a solar cycle. *Journal of Atmospheric and Terrestrial Physics*, *26*(1), 1–23. https://doi.org/10.1016/0021-9169(64)90104-7

Briggs, B. H. (1975). Ionospheric irregularities and radio scintillations. *Contemporary Physics*, *16*(5), 469–488. https://doi.org/10.1080/00107517508210825

Briggs, B. H., & Parkin, I. A. (1963). On the variation of radio star and satellite scintillations with zenith angle. *Journal of Atmospheric and Terrestrial Physics*, *25*(6), 339–366. https://doi.org/10.1016/0021-9169(63)90150-8

DasGupta, A., Ray, S., Paul, A., Banerjee, P., & Bose, A. (2004). Errors in position-fixing by GPS in an environment of strong equatorial scintillations in the Indian zone. *Radio Science*, *39*(1), 1–8. https://doi.org/10.1029/2002RS002822

De Forest, L. (1913). Recent developments in the work of the federal telegraph company. *Proceedings of the Institute of Radio Engineers*, *1*(1), 37–51. https://doi.org/10.1109/JRPROC.1913.216569

Dungey, J. W. (1956). Convective diffusion in the equatorial F region. *Journal of Atmospheric and Terrestrial Physics*, *9*(5–6), 304–310. https://doi.org/10.1016/0021-9169(56)90148-9

Felux, M., Circiu, M. S., Lee, J., & Holzapfel, F. (2017). Ionospheric gradient threat mitigation in future dual frequency GBAS. *International Journal of Aerospace Engineering*, *2017*(326018), 1–10. https://doi.org/10.1155/2017/4326018

Gladek, Y. C., Sousasantos, J., Salles, L. A., Lima Filho, V. C., Vani, B. C., & Moraes, A. O. (2019). GPS Amplitude fading due to ionospheric scintillation near the equatorial ionospheric anomaly. In *AIAA scitech 2019 forum* (pp. 1–12). https://doi.org/10.2514/6.2019-0057

Haerendel, G., Eccles, J. V., & Çakir, S. (1992). Theory for modeling the equatorial evening ionosphere and the origin of the shear in the horizontal plasma flow. *Journal of Geophysical Researh*, *97*(A2), 1209–1223. https://doi.org/10.1029/91JA02226

Huang, C. S., Retterer, J. M., de La Beaujardiere, O., Roddy, P. A., Hunton, D. E., Ballenthin, J. O., & Pffaf, R. F. (2012). Observations and simulations of formation of broad plasma depletions through merging process. *Journal of Geophysical Research*, *117*(A2), 1–11. https://doi.org/10.1029/2011JA017084

Humphreys, T. E., Psiaki, M. L., & Kintner, P. M. (2010). Modeling the effects of ionospheric scintillation on GPS carrier phase tracking. *IEEE Transactions on Aerospace and Electronic Systems*, *46*(4), 1624–1637. https://doi.org/10.1109/TAES.2010.5595583

Kintner, P. M., Kil, H., Beach, T. L., & de Paula, E. R. (2001). Fading timescales associated with GPS signals and potential consequences. *Radio Science*, *36*(4), 731–743. https://doi.org/10.1029/1999RS002310

Li, K. F., Lin, L. C., Bui, X. H., & Liang, M. C. (2018). The 11 year solar cycle response of the equatorial ionization anomaly observed by GPS radio occultation. *Journal of Geophysical Research: Space Physics*, *123*(1), 848–861. https://doi.org/10.1002/2017JA024634

Monico, J. F. G., Camargo, P. O., Alves, D. B. M., Shimabukuro, M. H., Aquino, M., Pereira, V. A. S., & Vani, B. C. (2013). From CIGALA to CALIBRA: An infrastructure for ionospheric scintillation monitoring in Brazil. In *AGU Meeting of Americas in Cancun*.

Moraes, A. O., Costa, E., Abdu, M. A., Rodrigues, F. S., de Paula, E. R., Oliveira, K., & Perrella, W. J. (2017). The variability of low-latitude ionospheric amplitude and phase scintillation detected by a triple-frequency GPS receiver. *Radio Science*, *52*(4), 439–460. https://doi.org/10.1002/2016RS006165

Moraes, A. O., Muella, M. T., de Paula, E. R., de Oliveira, C. B. A., Terra, W. P., Perrella, W. J., & Meibach-Rosa, P. R. (2018). Statistical evaluation of GLONASS amplitude scintillation over low latitudes in the Brazilian territory. *Advances in Space Research*, *61*(7), 1776–1789. https://doi.org/10.1016/j.asr.2017.09.032

Moraes, A. O., Vani, B. C., Costa, E., Abdu, M. A., de Paula, E. R., Sousasantos, J., et al. (2018). GPS availability and positioning issues when the signal paths are aligned with ionospheric plasma bubbles. *GPS Solutions*, *22*(4), 1–12. https://doi.org/10.1007/s10291-018-0760-8

Paul, A., Roy, B., Ray, S., Das, A., & DasGupta, A. (2011). Characteristics of intense space weather events as observed from a low latitude station during solar minimum. *Journal of Geophysical Research*, *116*(A10), 1–17. https://doi.org/10.1029/2010JA016330

Portella, I. P., de O Moraes, A., da Silva Pinho, M., Sousasantos, J., & Rodrigues, F. (2021). Examining the tolerance of GNSS receiver phase tracking loop under the effects of severe ionospheric scintillation conditions based on its bandwidth. *Radio Science*, *56*(6), 1–11. https://doi.org/10.1029/2020RS007160

Ray, S., Bhowmik, U., & Das, A. (2014). Scintillation effects related to propagation geometry as applicable to Indian SBAS. In *2014 XXXIth URSI General Assembly and Scientific Symposium (URSI GASS)* (pp. 1–4). https://doi.org/10.1109/URSIGASS.2014.6929763

Reilly, M. H., Harnish, L. O., & Goodman, J. M. (1981). *Polarimetry studies of ionospheric modification by rocket boosters*. Naval Research Laboratory.

Rino, C. L. (1979a). A power law phase screen model for ionospheric scintillation: 1. Weak scatter. *Radio Science*, *14*(6), 1135–1145. https://doi.org/10.1029/RS014i006p01135

Rino, C. L. (1979b). A power law phase screen model for ionospheric scintillation: 2. Strong scatter. *Radio Science*, *14*(6), 1147–1155. https://doi.org/10.1029/RS014i006p01147

Ryle, M., & Hewish, A. (1950). The effects of the terrestrial ionosphere on the radio waves from discrete sources in the galaxy. *Monthly Notices of the Royal Astronomical Society*, *110*(4), 381–394. https://doi.org/10.1093/mnras/110.4.381

Saito, S., Yoshihara, T., & Fujii, N. (2009). Development of an ionospheric delay model with plasma bubbles for GBAS. In *Proceedings of the 2009 International Technical Meeting of the Institute of Navigation* (pp. 947–953).

Salles, L. A., Moraes, A. O., Vani, B. C., Sousasantos, J., Affonso, B. J., & Monico, J. F. G. (2021). A deep fading assessment of the modernized L2C and L5 signals for low-latitude regions. *GPS Solutions*, *25*(3), 1–13. https://doi.org/10.1007/s10291-021-01157-4

Salles, L. A., Vani, B. C., Moraes, A. O., Costa, E., & de Paula, E. R. (2021). Investigating ionospheric scintillation effects on multifrequency GPS signals. *Surveys in Geophysics*, *42*(4), 999–1025. https://doi.org/10.1007/s10712-021-09643-7

Sobral, J. H. A., Abdu, M. A., Takahashi, H., Taylor, M. J., de Paula, E. R., Zamlutti, C. J., et al. (2002). Ionospheric plasma bubble climatology over Brazil based on 22 years (1977–1998) of 630 nm airglow observations. *Journal of Atmospheric and Solar-Terrestrial Physics*, *64*(12–14), 1517–1524. https://doi.org/10.1016/S1364-6826(02)00089-5

Sousasantos, J., Abdu, M. A., Moraes, A. O., Vani, B. C., Silva, R. P., & Sobral, J. H. A. (2021). Long-lasting stagnant equatorial plasma bubble event and the related scintillation over the Brazilian region. *Advances in Space Research*, *68*(11), 4678–4690. https://doi.org/10.1016/j.asr.2021.08.040

Sousasantos, J., Moraes, A. O., Sobral, J. H. A., Muella, M. T. A. H., de Paula, E. R., & Paolini, R. S. (2018). Climatology of the scintillation onset over southern Brazil. *Annales Geophysicae*, *36*(2), 565–576. https://doi.org/10.5194/angeo-36-565-2018

Sreeja, V. V., Aquino, M., Forte, B., Elmas, Z., Hancock, C., De Franceschi, G., et al. (2011). Tackling ionospheric scintillation threat to GNSS in Latin America. *Journal of Space Weather and Space Climate*, *1*(1), 1–9. https://doi.org/10.1051/swsc/2011005

Thébault, E., Finlay, C. C., Beggan, C. D., Alken, P., Aubert, J., Barrois, O., et al. (2015). International geomagnetic reference field: The 12th generation. *Earth Planets and Space*, *67*(1), 1–19. https://doi.org/10.1186/s40623-015-0228-9

Vani, B. C., Moraes, A. O., Salles, L. A., Breder, V. H. F., dos Santos Freitas, M. J., Monico, J. F. G., & de Paula, E. R. (2021). Monitoring ionospheric scintillations with GNSS in South America: Scope, results, and challenges. In *GPS and GNSS Technology in Geosciences* (pp. 255–280). Elsevier. https://doi.org/10.1016/B978-0-12-818617-6.00012-3

Yang, Z., & Morton, Y. T. (2020). Low-latitude GNSS ionospheric scintillation dependence on magnetic field orientation and impacts on positioning. *Journal of Geodesy*, *94*(6), 1–15. https://doi.org/10.1007/s00190-020-01391-7

Yeh, K. C., & Liu, C. H. (1982). Radio wave scintillations in the ionosphere. *Proceedings of the IEEE*, *70*(4), 324–360. https://doi.org/10.1109/PROC.1982.12313

Yoon, M., Kim, D., & Lee, J. (2020). Extreme ionospheric spatial decorrelation observed during the March 1, 2014, equatorial plasma bubble event. *GPS Solutions*, *24*(47), 1–11. https://doi.org/10.1007/s10291-020-0960-x